Correspondence of below-threshold high-order-harmonic generation and frustrated tunneling ionization

Wei-Hao Xiong,[1] Xiang-Ru Xiao,[1] Liang-You Peng,[1,2,*] and Qihuang Gong[1,2]

[1]*State Key Laboratory for Mesoscopic Physics and School of Physics, Peking University; Collaborative Innovation Center of Quantum Matter, Beijing 100871, China*

[2]*Collaborative Innovation Center of Extreme Optics, Shanxi University, Taiyuan, Shanxi 030006, China*

(Received 19 January 2016; published 20 July 2016)

Among many of the nonlinear phenomena induced by strong laser pulses, two of the important processes are the harmonic generation and the creation of neutral atoms in the Rydberg states. We carry out a joint study of the below-threshold high-order-harmonic (BTH) generation and the production of low-lying Rydberg atoms driven by an intense few-cycle midinfrared laser pulse. Our results are based on the numerical solution to the three-dimensional time-dependent Schrödinger equation within the single active electron approximation and a semiclassical simulation. The yields of BTH and low-lying Rydberg atoms are found to have a similar carrier envelope phase dependence. We find that both processes can be faithfully described semiclassically in the deep tunneling regime. The trajectory analysis shows that these two processes share the same series of trajectories and can be simultaneously manipulated by the driving pulse shape. Our finding bridges the below-threshold high-order-harmonic generation and the frustrated tunneling ionization.

DOI: 10.1103/PhysRevA.94.013417

The interaction of a strong laser pulse with atoms leads to a variety of nonlinear phenomena, which have attracted intensive studies for many decades. The detailed studies of strong-field processes not only allow us to understand and control the nuclear and electronic dynamics, but also can provide us with new light sources in a broad frequency range [1–6]. As the first step to many intense-field phenomena, the electron can tunnel through the distorted Coulomb potential barrier suppressed by the intense electric field of the laser pulse. Due to the attractive long-range Coulomb potential and the reversal of the laser electric field, it is possible for the electron to stay in the bound state after tunneling in two typical processes: high-order-harmonic generation (HHG), and frustrated tunneling ionization (FTI) [7–10]. Both processes can be qualitatively understood by the well-known simple man's model [11–13].

As first studied by Nubbemeyer and co-workers [7], FTI refers to the creation of neutral atoms in the Rydberg states (after the electron tunneling), with a probability much higher than that of the HHG [14]. Landsman and co-workers [10] carried out a detailed study about the similarities and differences between HHG and the creation of the Rydberg atoms through the laser ellipticity dependence. They found that the two processes involve electrons tunneling at different time: in the HHG, electrons tunnel out after the peak of the electric field and then recombine with the core, while the *dominant* FTI electrons tunnel before the peak and do not come back to the core. In addition, it has been showed by Liu *et al.* [9] that FTI is related to the partial atomic stabilization observed in strong-infrared (IR) fields. From a detailed semiclassical analysis, they found that there are actually two different types of orbits for the creation of Rydberg atoms: directly launched into the elliptical orbits (type 1) or ejected after collisions with the core (type 2).

Recently, the below-threshold high-order-harmonic (BTH) generation has drawn much attention due to its promising applications as a coherent light source or frequency comb in the vacuum ultraviolet [1,15–20]. While the HHG in the high-energy regime can be well explained by the strong-field approximation, the mechanism of near-threshold high-order-harmonic generation is rather complicated, whose description must deal with the Coulomb force and the laser interaction on equal footing [21–27]. For near-threshold high-order harmonics, previous studies have showed the important roles played by the Coulomb states and the multiple return trajectories [24,27].

In this work, we perform a joint study of the creation of low-lying Rydberg atoms (mainly via type 2 orbits) and BTH generation through an *ab initio* quantum calculation by solving the 3D time-dependent Schödinger equation (TDSE) and a classical trajectory Monte Carlo simulation (CTMC) [24]. Unlike the large distinctions between the high-energy HHG and the *dominant* Rydberg atoms' creation through the tpye 1 orbits [10], we find a perfect correspondence between the generation of low-lying Rydberg atoms and BTHs. In particular, the yields of both processes have the same dependence of the carrier envelope phase (CEP) for a few-cycle midinfrared (mid-IR) laser. To investigate the underlying mechanism of this relationship, we analyze the trajectories of the electrons from the CTMC for both processes and identify a series of electron trajectories tunneling around the peak of the field which contribute to this similarity. This means that the electrons contribute to the BTH and the low-energy FTI electrons share very similar initial conditions and trajectories. Both yields change the same way when these trajectories are influenced by varying the CEP of the mid-IR pulse.

In the TDSE calculations, the harmonic spectrum is calculated by the Fourier transform of the dipole acceleration and the population of Rydberg states is computed by projecting the final electron wave function onto the bound states, computed independently up to the principal quantum $n = 26$. In the CTMC simulation, the harmonic spectrum is calculated by the

*liangyou.peng@pku.edu.cn; http://www.phy.pku.edu.cn/~lypeng/

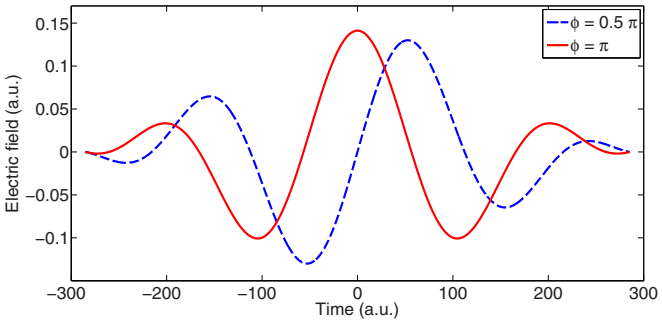

FIG. 1. Electric field of the driving laser for two different CEPs $\phi = 0.5\pi$ and $\phi = \pi$. The driving pulse is a 2.3-cycle $\sin^2$ pulse with a wavelength of 1800 nm and a peak intensity of 7×10^{14} W/cm^2.

method whose details can be found in our previous work [24]. The population in the Rydberg states from the CTMC method is calculated in the same way as many previous studies; e.g., see Refs. [9,14].

In the present study, a He atom in the single active electron approximation with a model potential given by $V(r) = -[1 + (1 + 27r/16)\exp(-27r/8)]/r$ [28] is shined by a few-cycle 1800 nm laser with the peak intensity of 7×10^{14} W/cm^2. The pulse has a total duration of 2.3 cycles for a $\sin^2$ pulse shape with a variable CEP. We show the electric field of the pulse in Fig. 1. As discussed in our previous work [24], the CEP effects can be clearly observed when the driving pulse is very short. The same CEP effects and the same correspondence relationship can be observed for a two or three cycle driving pulse, while for longer driving pulse, the CEP effects are not clear.

In Fig. 2, we first present a typical distribution of the Rydberg states (up to $n \sim 26$) created by the few-cycle mid-IR laser with the CEP $\phi = 0.6\pi$. The results of CTMC are normalized to those of the TDSE at $n = 2$. As pointed out by the previous study [9], there are two kinds of trajectories which contribute to the creation of the Rydberg atoms. For the present laser parameters, we find that these two kinds of electron trajectories are well separated by the final electron energy. Our calculations show that the electrons that end up in the high-lying Rydberg states ($n > 9$) never come back to the core after the tunneling. These majority electrons (type 1) will travel around the core after the end of the pulse

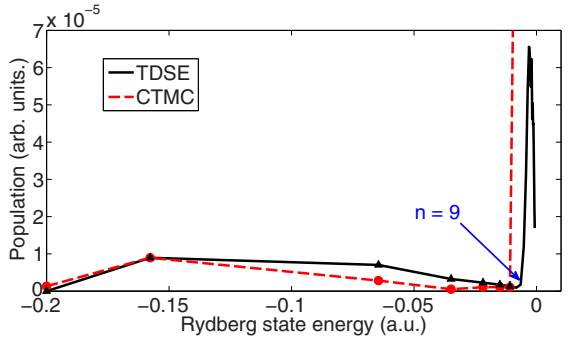

FIG. 2. Rydberg state population as a function of the electron energy, calculated by TDSE and CTMC, respectively, for the CEP $\phi = 0.6\pi$.

with a large radius. The CEP dependence of the populations for $n > 9$ is mainly determined by the ionization probability and it is not the main concern of the present work. Our investigation is mainly focused on the low-lying Rydberg states ($n \leqslant 8$), which originate from a different type of trajectory (type 2). These electrons will return to the vicinity of the core after the tunneling. Apart from being captured to the low-lying Rydberg states, they have a probability to emit BTH photons.

In the following, we will discuss the CEP dependence of the BTHs and the creation of the low-lying Rydberg atoms, emphasizing the underlying mechanism. We show that the electronic dynamics behind these two processes are very similar. In Fig. 3, we show the yields of BTHs (left column) and the Rydberg atoms (right column) as a function of the electron energy at different CEPs of the pulse, calculated by the TDSE and the CTMC, respectively. We subtract each harmonic energy by the value of the ionization potential I_p so that the horizontal axis of Figs. 3(a) and 3(c) stands for the return electron energy at its recombination instead of the photon energy. Besides, the Rydberg state population calculated by TDSE in Fig. 3(b) is represented by blocks in the energy axis because of the separated bound-state energies. We use the same energy blocks for the horizontal axis of all the other figures in Fig. 3 for a clear comparison of the CEP dependence. As one can see, the results from the CTMC simulations (lower panel) agree quite well with those of the TDSE calculations (upper panel). The striking feature is that the CEP dependence of BTHs and Rydberg state population is also very similar, both dominated in the CEP range of $(0.5\pi, 0.8\pi)$.

The CEP dependence for near-threshold high-order harmonics have been recently investigated in our previous paper [24], which can be explained by the half-cycle dynamics of the electrons. The half-cycle cutoff can extend to the low-energy regime for some certain CEPs. For the harmonics below the ionization potential, the electrons need at least one optical cycle to propagate before the recombination. Thus the electrons ionized close to the end of the pulse cannot reach such a low energy. At the same time, the ionization probability near the beginning of the pulse is rather small. The dominant signals between 0.5π and 0.8π can be understood roughly as follows: if the CEP increases, the ionization peak moves towards the beginning of the pulse and the ionization rate drops; if the CEP decreases, the ionization peak moves to the end of the pulse and the electrons do not have enough time to propagate and cannot generate low-energy electrons. For the population of the low-lying Rydberg states shown in Fig. 3(b) and Fig. 3(d), a similar CEP dependence as that of the BTH spectra can be observed. The main signals for the yield of Rydberg atoms are also observed for $\phi \in (0.5\pi, 0.8\pi)$. As we can see, the results from both methods agree with each other quite well. It is because the FTI process can be described from the classical description. This has been demonstrated by previous studies [7–10], although there are some arguments about the underlying mechanisms of stabilization process [29,30]. These observations indicate the similarity of the two processes and can be explained by the semiclassical model.

We first want to qualitatively understand the observed similarity of the CEP dependence of the two processes. From a classical point of view, we assume there are a series of

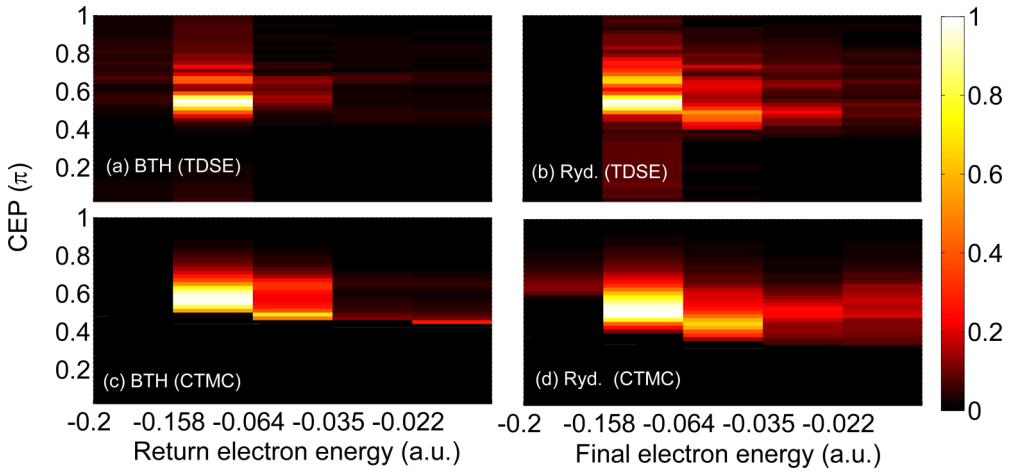

FIG. 3. Below-threshold high-order-harmonic spectra and the low-lying Rydberg state population, calculated respectively by TDSE [(a),(b)] and CTMC [(c),(d)], for different CEP ϕ of a 2.3-cycle $\sin^2$ pulse with a wavelength of 1800 nm and a peak intensity of 7×10^{14} W/cm^2.

electron trajectories contributing to both processes. The CEP of the driving pulse can influence the amount of this series of trajectories and then control the yields of BTH and Rydberg atoms at the same time. According to these features, we can have some preliminary understandings about these trajectories. The two restrictions for these electron trajectories are as follows: on the one hand, they should be able to return back to the core; on the other hand, they have negative total energies both when they return and when the pulse ends. These two restrictions can sketch the properties of these trajectories. For the first restriction, the electrons that end up in the Rydberg states are well separated by the final energy as type 1 and type 2 for the present laser wavelength. For the electrons contributing to the low-lying Rydberg atoms, they have the type 2 trajectory and will certainly return to the core after the tunneling. Thus the condition of returning to the core is satisfied for these electrons. For the second restriction, we know that the electrons which generate BTHs are mostly ionized at the peak of the driving field and return to the core after about one optical cycle. They do not gain much energy from the field during the traveling in the field and their total energies are negative when the recombination happens. The final momentum of the tunneled electron can be approximated by $p = -A(t)$, where $A(t)$ is the vector potential at the tunneling instant. Thus for the electrons that finally end up in the Rydberg states, they should get ionized when $A(t) \approx 0$, which is also around the peak of the electric field of the pulse.

To verify the above conjecture that the CEP dependence of those trajectories causes the similar CEP dependence of the two processes, we take the advantage of CTMC method to track the electron trajectories. The validity of the CTMC method for BTH has been shown in our previous paper [24]. Through the CTMC simulation, we verify the above assumption that the concerned electrons are indeed the returning electrons tunneling at the peak of the field. Specifically, these electrons tunnel out at the peak before the pulse center [for the ionization time and the field, see Fig. 5(b) for $\phi = 0.7\pi$]. For other CEPs, the ionization time changes from -50 a.u. to -100 a.u. when ϕ changes from 0.5π to 0.7π as we can see in Fig. 1. In the following, we can restrict our investigation to the electrons tunneling at this peak and show the electron motion with different initial conditions.

In the CTMC simulations, the ionization time is randomly sampled during the whole driving field. With the determination of ionization time, the initial positions and probabilities of the trajectories are determined according to the ADK theory [31]. The total ionization probability is

$$W(t_0, v_\perp^i) = W_0(t_0) W_1(v_\perp^i), \tag{1}$$

in which

$$W_0(t_0) \propto \left|(2I_p)^2/E(t_0)\right|^{2/\sqrt{2I_p}-1} \exp\left[-2(2I_p)^{3/2}/|3E(t_0)|\right]$$

determines the ionization rate with respect to the tunneling time and

$$W_1(v_\perp^i) \propto [\sqrt{2I_p}/|E(t_0)|] \exp\left[\sqrt{2I_p}(v_\perp^i)^2/|E(t_0)|\right] \tag{2}$$

gives the initial lateral momentum distribution, where $E(t)$ is the laser electric field and $v_\perp^i$ is the randomly sampled initial transverse momentum.

For the results shown in Fig. 3, the ionization time of the contributing electrons are mainly restricted to a single peak of the electric field. The electrons which tunnel out during this peak and that can return back to the core at a later time are ionized in a small time window of this peak. For a fixed driving pulse, the electron trajectories are determined by the ionization time, initial velocity, and initial position. However, when the ionization time is determined, the initial velocity and the tunneling probability are determined by the field strength. On the other hand, in the short time window we are concerned about, these two parameters do not change too much as the tunneling mainly happens in a single peak for a fixed CEP. Thus when we analyze the trajectories, the initial positions and ionization probabilities can be ignored. Therefore, the trajectories can be determined mainly by the ionization time and the initial perpendicular velocity.

In Figs. 4(a) and 4(c), we show the electrons' return energies at the recombination, as a function of the ionization time and the initial perpendicular velocity for $\phi = 0.6\pi$ and 0.7π, respectively. With the same initial conditions, we can

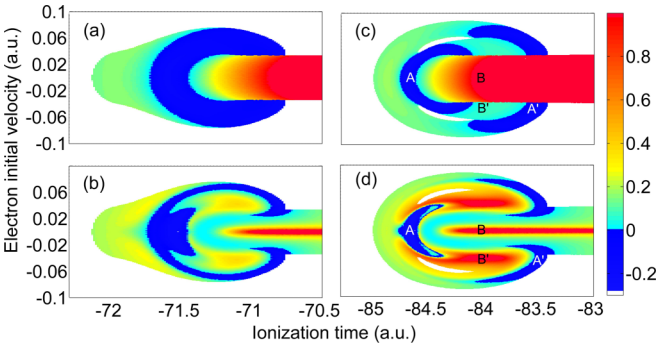

FIG. 4. Electron energies for electrons tunneling at the dominant peak of the electric field, as a function of the ionization time and the initial transversal momentum, for $\phi = 0.6\pi$ [(a),(b)] and 0.7π [(c),(d)], respectively: (a),(c) the electron energies at the recombination of the harmonics; (b),(d) the final electron energies at the end of the pulse.

also calculate the electron energies at the end of the laser pulse, as shown in Figs. 4(b) and 4(d). As the condition of returning to the core is satisfied when we calculate these trajectories, the negative final-energy electrons here are naturally type 2 electrons (contributing to low-lying Rydberg atoms).

We now discuss the details of the harmonic generation process in Figs. 4(a) and 4(c). First, the electron's initial perpendicular velocities are restricted in a certain range so that the electrons can recombine to the core. For the electron recombining at its first return, the perpendicular velocity should be no larger than 0.04 a.u. While for the second return, the electron's perpendicular velocity should be between 0.04 to 0.1 a.u., and the pulse is too short for higher-order returns. Secondly, for the usual high-order harmonics, the harmonic energy increases with the increasing time in this time window, as this time window is at the peak of the electric field where the long trajectory can be observed. Thirdly, when it comes to the near-threshold high-order harmonics (green areas), the corresponding electrons are very sensitive to the ionization times and initial perpendicular velocities, so the initial structures appear complicated. Along with the usual long trajectories extending to this energy range (about $t_i = -84.5$ a.u. for $\phi = 0.7\pi$), there are many other initial conditions contributing to these harmonics as well. These electrons, tunneling at the peak of the laser field with various initial conditions, can enhance the harmonics very close to the ionization threshold. The contribution of these electrons may be the reason for the observed harmonic emission around I_p [1].

We now turn to examining the final energies of the electrons as shown in Figs. 4(b) and 4(d). The final electron energy here can be understood roughly by $p = -A(t)$ together with the rescattering processes (regions marked as B and B′) caused by the ionic core. Here we mainly focus on the electrons related to the correspondence effect here. These electrons have a negative final energy [blue areas in Figs. 4(b) and 4(d)], corresponding to the negative recombination energy in the blue areas shown in Figs. 4(a) and 4(c). The blue areas in both Figs. 4(a) and 4(b) as well as Figs. 4(c) and 4(d) indicate those electrons with initial conditions in the following range: they have a negative total energy when they return to the core and also negative energies after the end of the pulse. This is the main reason for the observed proportional relationship between BTHs and the creation of the low-lying Rydberg atoms.

The CEP dependence of the yields can be interpreted from the comparison between the results of 0.6π and 0.7π. As we can see, when the CEP changes, the blue areas change accordingly. And it is not surprising that the blue areas for the recombination electron energy and the final electron energy keep the same shape for different CEPs. This is the reason that the two processes have the same CEP dependence. To analyze the yields of BTH and Rydberg atoms at different CEPs, we should consider both the size of the blue areas and the ionization probability (not included in this figure). When $\phi = 0.6\pi$, the size of blue areas is larger than that when $\phi = 0.7\pi$, and the ionization probability is also larger. This leads to a larger yield of both BTH and Rydberg atoms as shown in Fig. 3. For those CEPs in which case the BTH and FTI disappears, the electrons ionized at the peak of the field either cannot return to the core or have a small ionization probability, both of which processes are suppressed. Because of the sharing of the same series of trajectories, the yields of low-lying Rydberg atoms and BTHs can be controlled simultaneously through the manipulation of the driving pulse shape.

We can identify two separated blue areas contributing to BTH and low-lying Rydberg atoms when $\phi = 0.7\pi$ [marked as A and A′ in Figs. 4(c) and 4(d)]. To be more specific, we show their trajectories in Fig. 5. In Fig. 5(a), we present the electron position (distance to the core) as a function of time. Part of the 3D plot is shown in the inset. In Fig. 5(b), we show the time evolution of the electron energy. The electrons follow quite different trajectories for these two areas, though their initial conditions differ only a little and their final states are the same. The electron in the regime A gets ionized with a small velocity. When the driving field reverses, it returns to

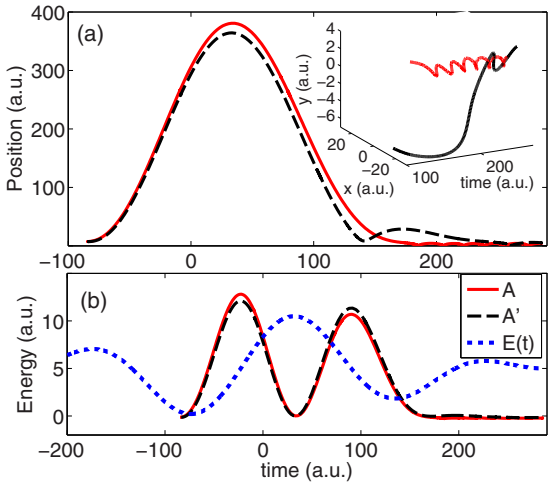

FIG. 5. Typical trajectories of electrons which generate BTHs and low-lying Rydberg atoms for $\phi = 0.7\pi$, whose initial condition corresponds to A and A′ marked in Fig. 4: (a) the electron position as a function of time; (b) the time evolution of the electron energy. Inset of (a) shows part of the 3D plot of the electron position.

the core and propagates very close to the core. If the electron velocity is small, it has a high chance to be trapped by the core. After its return, it circles near the core and never gets out again [see the inset in Fig. 5(a)]. For the electron in the regime A′, the initial velocity is relatively large. When it returns to the core for the first time, it is not close enough to the core. It has a probability to recombine at its second return with also a negative energy. Therefore, the two areas separate the electron trajectories by different travel times in the field.

To summarize, our study bridges the two important phenomena in strong-field physics. The yields of BTHs and low-lying Rydberg atoms are correspondingly investigated through a numerical solution to the TDSE and a CTMC simulation. Similar CEP dependence is observed in both processes. This phenomenon is explained by the similar initial condition of these two kinds of processes based on the trajectories of the CTMC.

This work is supported by National Natural Science Foundation of China (NSFC) under Grants No. 11574010 and No. 11322437, and by the National Program on Key Basic Research Project of China (973 Program) under Grant No. 2013CB922402. We acknowledge the critical reading and revision by Ji-Wei Geng.

[1] C. Gohle, T. Udem, M. Herrmann, J. Rauschenberger, R. Holzwarth, H. A. Schuessler, F. Krausz, and T. W. Hänsch, Nature (London) **436**, 234 (2005).
[2] F. Krausz and M. Ivanov, Rev. Mod. Phys. **81**, 163 (2009).
[3] M. Chini, K. Zhao, and Z. Chang, Nat. Photon. **8**, 178 (2014).
[4] T. Popmintchev *et al.*, Science **336**, 1287 (2012).
[5] A. Cingöz, D. C. Yost, T. K. Allison, A. Ruehl, M. E. Fermann, I. Hartl, and J. Ye, Nature (London) **482**, 68 (2012).
[6] L.-Y. Peng, W.-C. Jiang, J.-W. Geng, W.-H. Xiong, and Q. Gong, Phys. Rep. **575**, 1 (2015).
[7] T. Nubbemeyer, K. Gorling, A. Saenz, U. Eichmann, and W. Sandner, Phys. Rev. Lett. **101**, 233001 (2008).
[8] U. Eichmann, A. Saenz, S. Eilzer, T. Nubbemeyer, and W. Sandner, Phys. Rev. Lett. **110**, 203002 (2013).
[9] H. Liu, Y. Liu, L. Fu, G. Xin, D. Ye, J. Liu, X. T. He, Y. Yang, X. Liu, Y. Deng, C. Wu, and Q. Gong, Phys. Rev. Lett. **109**, 093001 (2012).
[10] A. S. Landsman, A. N. Pfeiffer, C. Hofmann, M. Smolarski, C. Cirelli, and U. Keller, New J. Phys. **15**, 013001 (2013).
[11] K. T. Kim, D. M. Villeneuve, and P. B. Corkum, Nat. Photon. **8**, 187 (2014).
[12] P. B. Corkum, Phys. Rev. Lett. **71**, 1994 (1993).
[13] M. Lewenstein, P. Balcou, M. Y. Ivanov, A. L'Huillier, and P. B. Corkum, Phys. Rev. A **49**, 2117 (1994).
[14] S. Eilzer and U. Eichmann, J. Phys. B **47**, 204014 (2014).
[15] D. C. Yost, T. R. Schibli, J. Ye, J. L. Tate, J. Hostetter, M. B. Gaarde, and K. J. Schafer, Nat. Phys. **5**, 815 (2009).
[16] E. P. Power, A. M. March, F. Catoire, E. Sistrunk, K. Krushelnick, P. Agostini, and L. F. DiMauro, Nat. Photon. **4**, 352 (2010).
[17] H. Soifer, P. Botheron, D. Shafir, A. Diner, O. Raz, B. D. Bruner, Y. Mairesse, B. Pons, and N. Dudovich, Phys. Rev. Lett. **105**, 143904 (2010).
[18] F. Brizuela, C. M. Heyl, P. Rudawski, D. Kroon, L. Rading, J. M. Dahlström, J. Mauritsson, P. Johnsson, C. L. Arnold, and A. L'Huillier, Sci. Rep. **3**, 1410 (2013).
[19] M. Chini, X. Wang, Y. Cheng, H. Wang, Y. Wu, E. Cunningham, P.-C. Li, J. Heslar, D. A. Telnov, S.-I. Chu, and Z. Chang, Nat. Photon. **8**, 437 (2014).
[20] A. K. Mills, T. J. Hammond, M. H. C. Lam, and D. J. Jones, J. Phys. B **45**, 142001 (2012).
[21] J. A. Hostetter, J. L. Tate, K. J. Schafer, and M. B. Gaarde, Phys. Rev. A **82**, 023401 (2010).
[22] J. Henkel, T. Witting, D. Fabris, M. Lein, P. L. Knight, J. W. G. Tisch, and J. P. Marangos, Phys. Rev. A **87**, 043818 (2013).
[23] K. Nasiri Avanaki, D. A. Telnov, and S.-I. Chu, Phys. Rev. A **90**, 033425 (2014).
[24] W.-H. Xiong, J.-W. Geng, Q. Gong, and L.-Y. Peng, New J. Phys. **17**, 123020 (2015).
[25] P. C. Li, Y. L. Sheu, C. Laughlin, and S.-I. Chu, Phys. Rev. A **90**, 041401(R) (2014).
[26] A. Spott, A. Becker, and A. Jaroń-Becker, Phys. Rev. A **91**, 023402 (2015).
[27] W.-H. Xiong, J.-W. Geng, J.-Y. Tang, L.-Y. Peng, and Q. Gong, Phys. Rev. Lett. **112**, 233001 (2014).
[28] D. R. Hartree, *Calculation of Atomic Structures* (Wiley, New York, 1957).
[29] K. C. Kulander, K. J. Schafer, and J. L. Krause, Phys. Rev. Lett. **66**, 2601 (1991).
[30] R. R. Jones and P. H. Bucksbaum, Phys. Rev. Lett. **67**, 3215 (1991).
[31] M. V. Ammosov, N. B. Delone, and V. P. Krainov, Sov. Phys. JETP. **64**, 1191 (1986).